Geophysical Research Letters

RESEARCH LETTER
10.1029/2020GL091913

Asian Emissions Explain Much of the Arctic Black Carbon Events

J. Backman[1], L. Schmeisser[2,3], and E. Asmi[1]

[1]Finnish Meteorological Institute, Atmospheric Composition Research, Helsinki, Finland, [2]University of Washington, Seattle, WA, USA, [3]National Oceanic and Atmospheric Administration, Earth Systems Research Laboratory, Boulder, CO, USA

Key Points:

- Black Carbon aerosols can travel from South Asia over Central Asia and to the Arctic in 7 days
- Black Carbon transported via this pathway measures well above the station average at almost all Arctic stations
- The identified pathway is significant for Black Carbon concentrations throughout the Arctic

Correspondence to:
J. Backman,
john.backman@fmi.fi

Citation:
Backman, J., Schmeisser, L., & Asmi, E. (2021). Asian emissions explain much of the Arctic Black Carbon events. *Geophysical Research Letters*, *48*, e2020GL091913. https://doi.org/10.1029/2020GL091913

Received 12 AUG 2020
Accepted 15 JAN 2021

Abstract There is ample evidence that Black Carbon (BC) is harmful to the Arctic. BC can darken the otherwise highly reflective surfaces of snow and ice and increase atmospheric and ice surface temperatures. Because of the importance of BC to the Arctic, this work was designed to resolve the most significant source regions of Arctic BC as measured by monitoring stations in the Arctic. Using a bottom-up approach, it is shown for the first time that there is one particular BC transport pathway from lower latitudes into the Arctic that registers at all but one of the Arctic surface monitoring stations included in this study. Through this pathway, pollutants are transported from the Indo-Gangetic plane over Central Asia into the high Arctic in as little as 7 days. The measurement sites and BC pathways in this study are shown to be well representative of the Arctic as a whole.

Plain Language Summary Snow and sea ice are two of the most reflective surfaces occurring naturally on planet Earth. Light absorbing aerosols, such as wind blown black carbon, that stick to these pristine surfaces can make them less reflective, thus converting more sunlight into heat. The added heat leads to increased surface temperatures and is detrimental to the Arctic climate. There are few sources of light absorbing aerosols in the Arctic compared to the vast amounts of black carbon aerosols that are emitted closer to the equator. This research highlights an important pathway for light absorbing aerosols to enter the Arctic. Light absorbing aerosols that enter the Arctic through this pathway can then subsequently spread out throughout the Arctic. This pathway is shown to transport light absorbing airborne pollutants from South Asia, over Central Asia, and into the high Arctic in quantities that well exceed the background levels, thus highlighting the importance of this newly found pathway.

1. Introduction

Black carbon (BC) aerosols contribute to the rapid warming of the Arctic (Sand et al., 2015; Serreze & Barry, 2011). Snow and sea ice are natural surfaces with very high albedo, reflecting much of the sun's energy back to space. However, when light absorbing impurities are present, the albedo can decrease substantially, and they convert sunlight into heat, thus increasing the surface temperature (Hansen & Nazarenko, 2003). Potent light absorbing impurities, such as BC, are found throughout the Arctic (Doherty et al., 2010), and end up in snow and ice sheets through atmospheric transport and subsequent deposition. The Arctic is particularly sensitive to changes in surface temperature, and increases in surface temperature are coupled to sea ice extent. Therefore, an increase in surface temperatures in the Arctic, through the coupling of sea ice and surface temperature, gives rise to Arctic amplification that is driven by heat transfer from open water instead of sea ice (Serreze & Barry, 2011). The effect of BC and soot on climate is not limited to albedo changes through deposition onto snow and ice, as suspended BC can also affect the temperature structure of the atmosphere by absorbing solar radiation in the air (Koch & Genio, 2010). Because BC is so destructive for the Arctic climate, it is essential to understand BC properties, transport to, and concentrations in the Arctic. Arctic warming has further been exacerbated by the reduction of sulphur emissions in the northern hemisphere, thus fueling Arctic amplification (Navarro et al., 2016; Mauritsen, 2016). During the last decade, vast amounts of Arctic sea ice volume have been lost and multiyear sea ice is at an alltime low (Serreze & Stroeve, 2015; Serreze & Meier, 2018). The potential of BC to perturb surface temperatures in the Arctic makes measurements of BC particularly important.

Long term surface concentrations of BC in the Arctic have mostly decreased during the 1990s and 2000s (Hirdman, Burkhart, et al., 2010; Sharma et al., 2013). Recently, this trend seems to have leveled off with little to no trend observed for surface level BC in the Arctic during the last decade based on a trend analysis including all seasons (Coen et al., 2020). However, higher up in the Arctic atmosphere the situation might be different as East Asia is expected to contribute more substantially to the BC levels at higher altitudes (Ikeda et al., 2017; Sharma et al., 2013). It has been shown that emissions within the Arctic itself, such as those from gas flaring, have the potential to increase local BC surface levels substantially (Stohl et al., 2013), but this is not necessarily true for the whole Arctic (Winiger et al., 2017).

Research suggests that the seasonality of BC in the Arctic is less sensitive to annual variations of emissions than to annual changes in transport patterns of BC into the Arctic (Chen et al., 2020; Willis et al., 2018). Seasonal changes in removal processes are another known source of the seasonality of Arctic aerosols (Garrett et al., 2011). The day-to-day variability of BC in the Arctic is best modeled with high temporal resolution of BC emissions, while annual variability is best reproduced with static emissions (Schacht et al., 2019). Moreover, possible misallocations of emissions between biomass and fossil fuel sources in emissions inventories can lead to misleading results when modeling the relative importance of natural and anthropogenic sources of BC (Winiger et al., 2019). Emissions from domestic burning and wildfires are important for further constraining the impacts of BC on the Arctic (Winiger et al., 2019) and the inclusion of open biomass burning improves modeled Arctic BC (Winiger et al., 2017). Improved emissions inventories would also help to reproduce measured levels of BC that models tend to underestimate, particularly during winter and spring (Eckhardt et al., 2015).

In this work, the uncertainties associated with emissions inventories are circumvented with a focus on in-situ measurements of surface BC concentrations from multiple Arctic sites, standardized into one data set that is post processed to achieve a much better detection limit than what has been used in previous studies (Backman et al, 2017b). Using these measurements, we ask which source region is the largest contributor to Arctic BC concentrations; that is where does BC measured at a select six Arctic stations come from? The aim of this study is therefore to provide a bottom-up estimate of the annual Arctic BC source regions using the best available long-term data sets.

A widely used means of measuring BC is by filter-based absorption photometry, which yields light absorption coefficients (σ_{ap}) that are related with equivalent BC (eBC) mass concentration – a variable often used for modeling purposes (Petzold et al., 2013). In this work σ_{ap} are reported, as this is what the absorption photometers actually measure. Given their importance in the Arctic, this study is focused on, but not restricted to, light absorbing aerosols. This work expands on previous work that involved data processing, data quality control, and interpretation of aerosol optical properties at six Arctic stations (Backman et al., 2017a; Schmeisser et al., 2018). The data set used here has been published previously (Backman et al., 2017b).

2. Materials and Methods

Lagrangian trajectory models are widely used to investigate source-receptor relationships of atmospheric constituents based on air-mass movement from meteorological data in grid form (Rastigejev et al., 2010). The method involves the calculation of an air parcel's movement from the receptor site, back in time, which yields the back trajectory of the virtual parcel of air (Stein et al., 2015).

The HYSPLIT model was run 7 days back in time using the ensemble method. The ensemble method will offset the meteorological grid by one grid point in the horizontal and 1% of the surface pressure level in the vertical. This will produce 27 back trajectories for all possible offsets in the horizontal and vertical, thus accounting for uncertainties in the meteorological data grid. The meteorological data used for the trajectories was the NCEP/GDAS data set with a 1° horizontal resolution with 23 pressure levels (Kanamitsu, 1989).

The back trajectory analysis was executed by combining the measured aerosol property (c) at one of the sites (s) at time (t) with back-trajectories as given by the HYSPLIT model for that point in time. Back-trajectories were calculated for all sites and all times when there were measurement data available. For a given t (and s), the calculated back trajectory path was matched with grid points (g) in a geodesic grid that had been closest to that back trajectory. Those grid cells were associated with $c(s, t = i)$ so that a weighted arithmetic

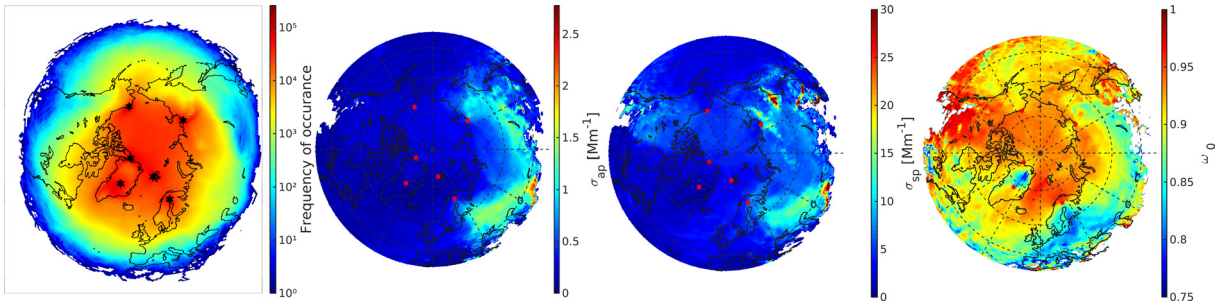

Figure 1. (a) Heat map of the amount of back trajectory overpasses for the study period 2012–2014. The calculated back trajectories extend 7 days back in time. Also shown are the abbreviations used for the stations: Alert (ALT), Barrow (BRW), Pallas (PAL), Summit (SUM), Tiksi (TIK), and Zeppelin (ZEP). Footprints of aerosol optical properties combining data from six Arctic stations showing (b) aerosol light absorption σ_{ap}, (c) aerosol light scattering σ_{sp}, and (d) shows aerosol single scattering albedo (ω_0).

mean ($\overline{c}_g$) could be calculated for each grid cell. While matching back-trajectories with grid points (g) and measurements (c), the distance traveled (d) from the site (s) was also calculated and used for weighing (w) the arithmetic means for each of the grid points. Given that there were N overpasses of a grid point g then $\overline{c}_g$ is calculated as

$$\overline{c}_g = \sum_{i=1}^{N} c(t,s)_i w(d,s)_i \; / \; \sum_{i=1}^{N} w(d,s)_i \tag{1}$$

This equation describes how the footprint maps were calculated. The weights in Equation 1 were the inverse distance traveled from the receptor point along the trajectory path. Thus, the receptor location closest (in traveled distance) to a grid cell would weigh the grid cell highest. This follows the rationale that the station closest to a grid cell is the most representative since removal processes and dilution reduce the pollutants as they are advected away from the source. Furthermore, uncertainties in the trajectory path increase with distance traveled. Trajectory points less than 500 m above ground level were considered in the analysis. This corresponds to the two lowermost pressure levels in the meteorological input data.

The aerosol properties (c) investigated in this work are light absorption coefficients σ_{ap} that can be converted into BC mass concentrations, light scattering coefficients σ_{sp}, and single scattering albedo ω_0.

3. Results

3.1. Footprints of Aerosol Optical Properties

The advection analysis was conducted using the Hybrid Single-Particle Lagrangian Integrated Trajectory model (HYSPLIT) version 4.9 (Stein et al., 2015) and the National Center for Environmental Prediction Global Data Assimilation System (NCEP GDAS) meteorological data (Kanamitsu, 1989). The advection model output, in the form of back trajectories, was used to calculate footprints based on measurements of σ_{ap} at the six Arctic stations (Figure 1). The back trajectories were matched with aerosol optical properties measured at the receptor sites and those properties were assigned to traversed grid cells according to the back trajectories to construct a map of origin of the measured properties (referred to here as a footprint map). In addition to σ_{ap}, footprints of light scattering coefficients (σ_{sp}) and single-scattering albedo (ω_0) are also calculated; ω_0 was calculated as $\sigma_{sp}/(\sigma_{sp} + \sigma_{ap})$). The aerosol optical properties data set is comprised of three years of standardized data from 2012 to 2014. Detailed site descriptions, data processing methods, and the data have all been published elsewhere previously (Backman et al., 2017a, 2017b; Schmeisser et al., 2018). The measurement data are reported at a wavelength of 700 nm.

The source region density map of the back trajectories and the footprints of the aerosol properties are depicted in Figure 1. Figure 1a shows the number of trajectories that have passed a particular grid point and Figures 1b–1d show the weighted means of the measured variables. In other words, Figures 1b–1d should be interpreted in combination with Figure 1a, which shows the number of trajectories that have passed a particular grid point. From Figure 1a it is evident that the six stations included in this study together cover

the Arctic and the northern Eurasian and American continents, with decreasing influence from the mid- and low latitudes. Figure 1a also shows the underlying geodesic grid to which the measured properties were averaged to avoid poor statistics for grid cells close to the pole.

Figure 1b shows the σ_{ap} footprint map following the rationale of the methods section. In general, for σ_{ap}, it can be said that the footprint map shows very low concentrations for the whole Arctic region. In the east, namely Central Asia, elevated concentrations of light absorbing aerosols are clearly visible compared to higher latitudes with low concentrations over the Arctic ocean and the Norwegian sea. This is expected since there are few sources of light absorbing aerosols over the oceans in general and especially in the Arctic since little human activity is expected on sea ice. When air masses are advected over the Arctic measurement stations from polluted areas in Asia in under 7 days, the probability of measuring high levels of light absorbing aerosols (i.e., above station mean values) clearly increases. This suggests a substantial contribution of Asian emissions to BC levels in the Arctic, and thus also σ_{ap}.

The more densely populated areas of Europe and North America do not stand out on the map as one might expect. This could be due to a couple of factors. First, no deposition or scavenging were accounted for in producing Figure 1, so an increased distance to the source areas would therefore decrease the importance of distant sources. The proximity of a source to the high Arctic has been shown to increase surface concentrations substantially, which is the case for gas flaring from locations close to or within the Arctic (Stohl et al., 2013). Second, the geographical distance itself does not constitute the only variable for a source's ability to affect the Arctic. Atmospheric circulation patterns also play a significant role (Chen et al., 2020; Stohl, 2006). Some stations, namely SUM in this work, do not seem to receive the same air-masses as the other stations. This is most likely due to air-mass movement and the unique topography of the station's surroundings (Hirdman, Sodemann, et al., 2010; Schmeisser et al., 2018). Moreover, precipitation patterns, and therefore aerosol wet-scavenging, can affect the amount of aerosols transported into and within the Arctic. The fact that the Asian mid-latitudes stand out as a source region of BC suggests that these aerosols are indeed transported into the Arctic.

The continental land areas also stand out in the footprint for σ_{sp} (Figure 1c). For the Arctic ocean and the Norwegian sea, a similar homogeneity is observed as was the case for σ_{ap}. There is no clear difference between the high Arctic ocean and oceans at lower latitudes. What is apparent, though, is that more scattering aerosols seem to originate from over land than from over presumably open water. This is true for the areas over Russia, and to some extent, North America. Also visible, but to a lesser extent, is the area also associated with elevated light absorbing aerosols (southern and south of Siberia). The seas that do not freeze over during winter do not stand out as a source of scattering sea salt aerosols. The Arctic ocean should only be a source of sea salt aerosols to the extent that the sea ice melts during summer.

The footprint of ω_0 shows that the marine regions are associated with brighter aerosols ($\omega_0 = 0.93–0.96$) while lower ω_0 values are observed over the continents (Figure 1d). The lower ω_0 values over land do not hold true, however, for the western part of North America. The ω_0 over Europe is lower than over the Norwegian sea and the Arctic ocean. This is expected as combustion aerosols with low ω_0 are found in continental Europe in much greater quantities than over the oceans. If the scavenging and dilution processes are similar for light absorbing and light scattering aerosols, which is likely for long-rage transported submicron aerosols, then the ω_0 should be a better reflection of differences in aerosol types than the extensive aerosol properties of σ_{ap} and σ_{sp}. At lower latitudes, below 60 °N, the ω_0 footprint becomes less uniform, which is likely due to fewer data points in the figure; see Figure 1a.

It has been shown that SUM receives different air-masses than the other stations (Schmeisser et al., 2018). The ω_0 can also drop well below 0.9 in late summer which is the reason for the low ω_0 over northern Greenland Hirdman, Sodemann, et al., 2010; Schmeisser et al., 2018). It seems unlikely that the source of the low ω_0 would be from Greenland; rather, it is more probable that the source is further away and beyond the transport times investigated in this study. The characteristically different air masses arriving at SUM are due to the fact that SUM is the only high altitude station and is located on top of the Greenland ice shelf.

The 7-day back trajectory was a compromise between having a time period long enough to be able to include distant sources in the analysis and short enough so that the trajectories are still trustworthy. The 7-day duration is also the time scale that could be expected for e-folding lifetime of typical BC-containing atmospheric

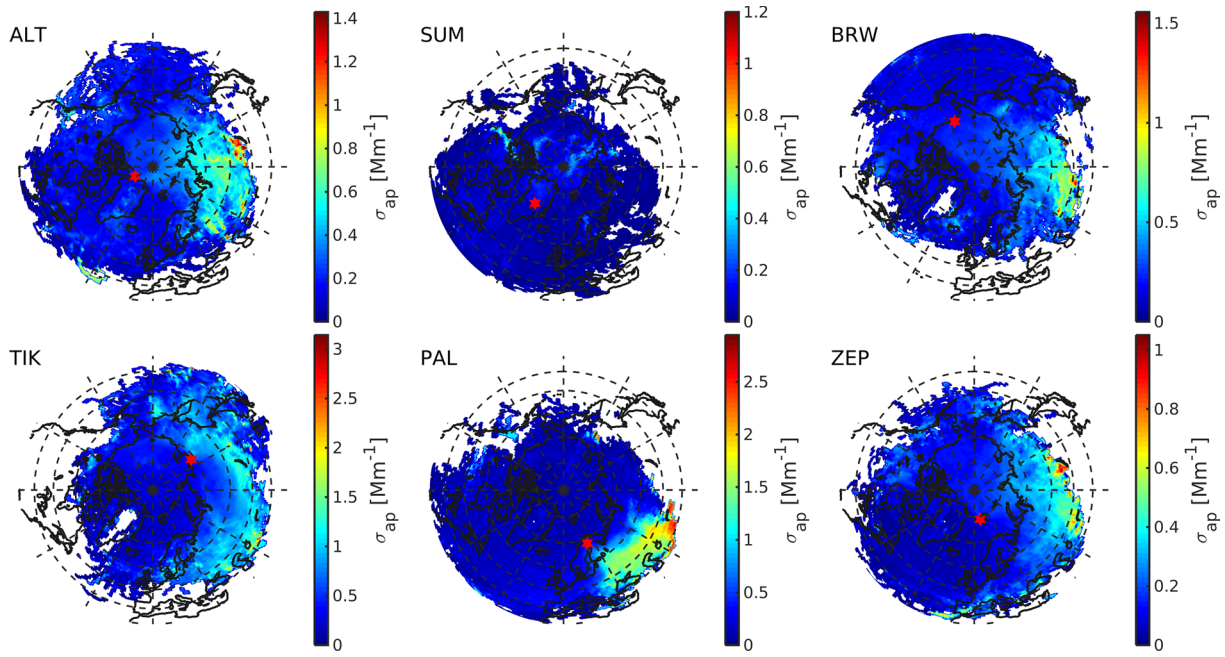

Figure 2. Individual footprints of σ_{ap} for the respective sites. Note that the color bar differs from site to site to make the individual features more clear.

aerosols (Raes et al., 2000). Some parts of the aerosol-laden areas in Asia could be beyond the reach of the 7-day transport time that has been modeled here. If the modeled long-range transport exceeds 7 days, then the edge of the model domain would be associated with elevated concentrations in that area. This is indeed the case for the earlier discussed elevated values of σ_{ap} over Central Asia; i.e. east of the Caspian Sea. Evidence of this is discussed in the next section with the aid of emissions inventories.

The multiple trajectory approach of HYSPLIT was chosen to include the uncertainty in the meteorological data fields (Stein et al., 2015). In the chosen modeling approach, the footprint represents the areas that are relatively important as sources of aerosols in the Arctic rather than the absolute amount of aerosols released at the source. If interest lies in the absolute amount at the source, then accounting for deposition and dilution during transport would be essential. Several studies have shown that modeling these processes in the Arctic is challenging, which in turn makes source apportionment uncertain (Willis et al., 2018).

3.2. Source Areas

Figure 2 shows the site specific footprints for σ_{ap}. Results for all stations except SUM show elevated concentrations of light absorbing aerosols arriving from central Asia; although the absolute concentrations differ (Figure 2). A difference in absolute levels is expected because of the different paths (and therefore removal and dilution processes) that the aerosols have been subject to before arriving at the stations. This consistency in independent station-specific results gives confidence for the overall conclusions of this study. Moreover, it implies that the same source area is not only important for single stations but for a greater portion of the Arctic as well.

Emissions of the pollutants measured at the Arctic stations are plotted in Figure 3. These include anthropogenic BC and PM10 emissions from the ECLIPSE (Evaluating the CLimate and Air Quality ImPacts of ShortlivEd Pollutants) v5 emission inventory (Klimont et al., 2017) and BC emissions from Savanna, Boreal, Temperate forests, tropical deforestation, peat and agricultural fires from the Global Fire Emissions Database GFED4s (Randerson et al., 2017). The BC emissions in the ECLIPSE and GFED inventories should both increase σ_{ap} levels if present in air-masses arriving at the respective stations, whereas PM10 emissions would show up in elevated σ_{sp} levels. As wildfires not only produce light absorbing aerosols but also light scattering aerosols, forest fires also register as elevated σ_{sp}.

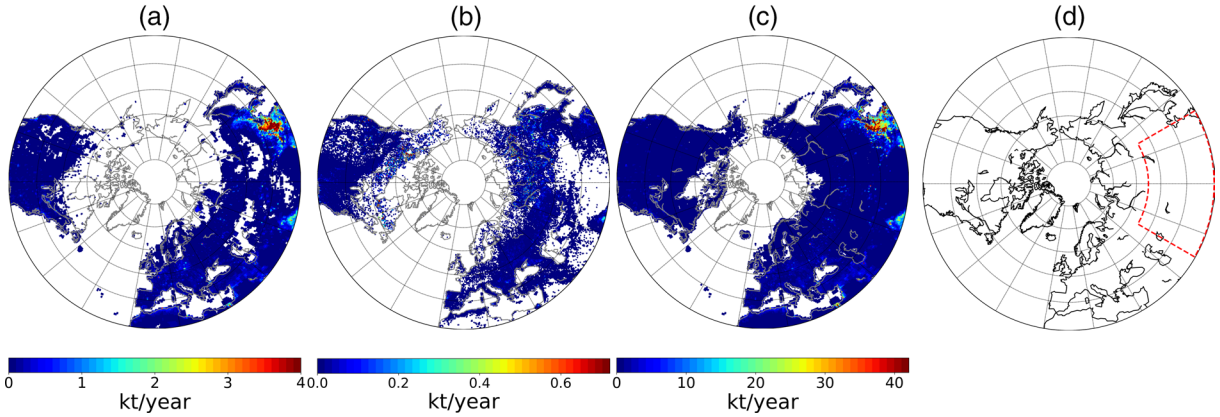

Figure 3. The figure shows (a) Evaluating the CLimate and Air Quality ImPacts of ShortlivEd Pollutants (ECLIPSE) v5 black carbon emissions, (b) Global Fire Emissions Database (GFED4s) emissions of carbon from wildfires, and (c) ECLIPSE v5 PM_{10} emissions, and (d) the source area for the time series analysis. To represent the measurement period of 2012–2014 the ECLIPSE data are a mean of the years 2010 and 2015 and the GFED4s data are a mean of the years 2012–2014.

The emission maps of Figure 3 show some of the features of the footprint maps in Figure 1. The BC emissions (ECLIPSE + GFED) show the same general pattern as the σ_{ap} footprint depicts (Figure 1). Over Russia the σ_{ap} footprint shows elevated concentrations corresponding to the GFED wildfire areas. The source area east of the Caspian Sea (Central Asia) that was discussed earlier is also visible on the emission inventory maps. However, those sources are further south in northern Pakistan and India, whereas the footprints of Figure 1 show the source area to be farther north. This supports our earlier hypothesis that source areas outside of the modeled 7-day travel time would show up at the edges of the footprint maps if the sources farther away are strong enough.

The eastern parts of China do not stand out in the σ_{ap} footprint (Figure 1b). These areas are clearly heavily polluted according to the emission inventory maps in Figure 3a. This implies that light absorbing aerosols from those areas do not end up in the Arctic as easily as those that originate south of Central Asia, which holds true for all the six measurement stations and supports previous research (Sharma et al., 2013). TIK, the closest station to East Asia, does not show an abundance of light absorbing aerosols originating from the eastern China region. ALT, BRW and ZEP do show elevated σ_{ap} levels from over Asia but not from the eastern China area which is associated with high emissions in the ECLIPSE emission inventory maps.

The footprint analysis does not show the time of the individual pollution events that knowingly registered at the different stations. Thus, it is unclear whether the stations observe the same or separate events. Therefore, back trajectories that traversed the Central Asian "hot spot" and entered the Arctic were investigated to see if the associated events occur concurrently at the respective stations. The hot spot area is shown in Figure 3d and the results confirm that several events are detected at all or several of the low altitude stations. Figure 4 shows the time series of σ_{ap} with the periods when air masses originate from inside the square in Figure 3d marked with black dots.

Events occur so that ALT, BRW, PAL, TIK and ZEP concentrations peak for extended periods of time when receiving air-masses from the area shown in Figure 3d. PAL is the station with the clearest peaks and the longest duration of air masses coming from that area and is clearly visible in the site specific footprint (Figure 2). TIK is most frequently influenced by the hot spot area due to its geographical proximity. A carbon isotope source-apportionment study of BC containing aerosols at Tiksi concluded that biomass burning aerosols were dominant during low concentrations in summer and fossil fuel was dominant during the Arctic haze period (Winiger et al., 2017). The concentrations shown for TIK in Figure 4 follow the same annual cycle as the isotope study and during the Arctic haze period much of the air mass originates from within the box. Moreover, since forest fires do not occur during the Arctic winter, the BC sources within the box should be anthropogenic in origin, at least during the winter. Unsurprisingly, SUM is again the outlier, as the station experiences virtually no periods with air originating within the selected area.

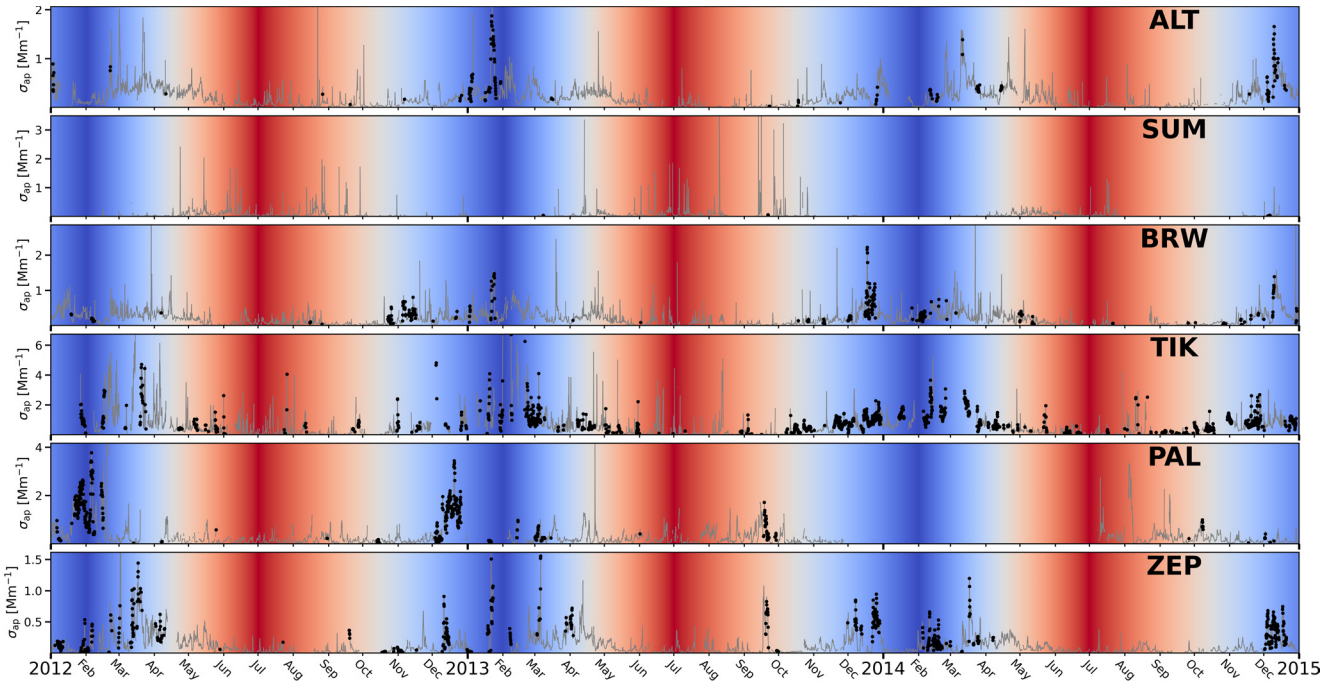

Figure 4. Time series of σ_{ap} for the respective stations with the time periods when trajectories have traversed the area shown in red in Figure 3d marked with black dots. The background color depicts the seasons from midwinter in February (blue) to high summer in July (red).

4. Conclusions

There is ample evidence that black carbon (BC) aerosols are detrimental for the Arctic climate. Modeling BC in the Arctic has improved, but models still struggle to replicate the seasonality and concentration of measured levels of pollution (Eckhardt et al., 2015; Sato et al., 2016; Willis et al., 2018). This seasonality is also evident in our data set, which shows that the BC concentrations are the lowest during summer (Schmeisser et al., 2018).

This unique three year data set of Arctic aerosol optical properties, including light absorption and scattering, was used as a base in the bottom-up modeling approach designed to resolve the most significant Arctic aerosol source regions. The source-area analysis using back trajectories is a simple yet effective technique for pinpointing important regions that contribute to increased levels of light absorbing aerosols, such as BC, in the Arctic. The analysis was, in a general way, able to reproduce the spatial pattern of emissions in the emission datasets, providing confidence for the chosen analysis method (Figures 1 and 3). Figure 1 shows elevated concentrations of light absorbing aerosols over Central Asia, which frequently register at all low altitude monitoring stations and far exceed background levels Figure 4.

There are two very clear pollution hot spots in Asia-the Indo-Gangetic Plain and Eastern China (Gustafsson & Ramanathan, 2016). Out of these two, pollution from the Indo-Gangetic Plain is shown to be far more likely to end up in the Arctic than has previously been shown. The analysis shows that there is measurement-based evidence of this major pathway, which frequently contributes to elevated levels of light absorbing aerosols throughout the Arctic. This source area shows up in all low altitude Arctic monitoring stations included in this study. Furthermore, the pathway identified does not contribute to isolated events of pollution for the individual sites but shows up in multiple measurements stations at the same time, indicating that the pollution intrusions spread out over wide areas in the Arctic. For at least half of the stations, these bursts far exceed seasonal levels of increased light absorbing aerosols common in the Arctic during winter months.

BC measurements provide invaluable proof of whether or not mitigation strategies work and, furthermore, are paramount for showing how well models are able to represent aerosols in the Arctic. This work clearly indicates that one important transport pathway of light absorbing aerosols into the Arctic is from central

Asia. In order to properly model Arctic aerosols, transport pathways like those found here will have to be represented in models.

Data Availability Statement

ALERT data are from Environment and Climate Change Canada, Sangeeta Sharma, technicians and operators, and the Canadian Department of National Defense. BARROW data are from Patrick Sheridan, and Elisabeth Andrews (NOAA Earth System Research Laboratories/GML). SUMMIT data are from Patrick Sheridan and Elisabeth Andrews (NOAA Earth System Research Laboratories/GML), Michael Bergin (Duke University), and the National Science Foundation (OPP 1546002). TIKSI data are from Sara Morris (NOAA Earth System Research Laboratories/GML/PSL) and the Academy of Finland project Greenhouse gas, aerosol and albedo variations in the changing Arctic (project number 269095). PALLAS data are from the Academy of Finland project Greenhouse gas, aerosol and albedo variations in the changing Arctic (project number 269095), the Academy of Finland project Novel Assessment of Black Carbon in the Eurasian Arctic: From Historical Concentrations and Sources to Future Climate Impacts (NABCEA), project number 296302, and the Academy of Finland Centre of Excellence Programme (project number 307331). ZEPPELIN data are from the Swedish Environmental Protection Agency (Naturvrdsverket), Vetenskaprdet, FORMAS, NILU (Norsk institutt for luftforskning), and Peter Tunved (Stockholm University). Data management is provided by WMO's Global Atmosphere Watch World Data Centre for Aerosol.

The HYSPLIT model is freely available for the scientific community upon registration at http://www.ready.noaa.gov/HYSPLIT.php.

The Meteorological data for the model are provided by National Weather Service's National Centers for Environmental Prediction (NCEP) Global Data Assimilation System (GDAS) and is only available at the ftp link at ftp://arlftp.arlhq.noaa.gov/pub/archives/gdas1

The ECLIPSE v5 global emission fields are publicly available at https://iiasa.ac.at/web/home/research/researchPrograms/air/ECLIPSEv5.html. The GFED4s data can be accessed here http://www.globalfiredata.org/data.html.

Acknowledgments
This project has received funding from the European Union's Horizon 2020 research and innovation program under grant agreement No. 654109 (ACTRIS). The authors acknowledge the Aerosol working group of the International Arctic System for Observing the Atmosphere (IASOA) for coordinating the data and expert contributions that led to the publication of the measurement data set.

References

Backman, J., Schmeisser, L., Virkkula, A., Ogren, J. A., Asmi, E., Starkweather, S., et al. (2017a). On aethalometer measurement uncertainties and an instrument correction factor for the arctic. *Atmospheric Measurement Techniques*, *10*(12), 5039–5062. https://doi.org/10.5194/amt-10-5039-2017

Backman, J., Schmeisser, L., Virkkula, A., Ogren, J. A., Asmi, E., Starkweather, S., et al. (2017b). *Time series of aerosol light-absorption coefficients from aethalometers at six arctic stations between 2012 and 2014NILU – Norsk Institutt for Luftforskning*. https://doi.org/10.21336/gen.1

Chen, X., Kang, S., & Yang, J. (2020). Investigation of distribution, transportation, and impact factors of atmospheric black carbon in the arctic region based on a regional climate-chemistry model. *Environmental Pollution*, *257*, 113127. https://doi.org/10.1016/j.envpol.2019.113127

Collaud Coen, M., Andrews, E., Alastuey, A., Arsov, T. P., Backman, J., Brem, B. T., et al. (2020). Multidecadal trend analysis of aerosol radiative properties at a global scale. *Atmospheric Chemistry and Physics*, *20*(14), 8867–8908. https://doi.org/10.5194/acp-20-8867-2020

Doherty, S. J., Warren, S. G., Grenfell, T. C., Clarke, A. D., & Brandt, R. E. (2010). Light-absorbing impurities in arctic snow. *Atmospheric Chemistry and Physics*, *10*(23), 11647–11680. https://doi.org/10.5194/acp-10-11647-2010

Eckhardt, S., Quennehen, B., Olivié, D. J. L., Berntsen, T. K., Cherian, R., Christensen, J. H., et al. (2015). Current model capabilities for simulating black carbon and sulphate concentrations in the arctic atmosphere: A multi-model evaluation using a comprehensive measurement data set. *Atmospheric Chemistry and Physics*, *15*(16), 9413–9433. https://doi.org/10.5194/acp-15-9413-2015

Garrett, T. J., Brattström, S., Sharma, S., Worthy, D. E. J., & Novelli, P. (2011). The role of scavenging in the seasonal transport of black carbon and sulphate to the arctic. *Geophysical Research Letters*, *38*, L16805. https://doi.org/10.1029/2011GL048221

Gustafsson, Ö., & Ramanathan, V. (2016). Convergence on climate warming by black carbon aerosols. *Proceedings of the National Academy of Sciences*, *113*(16), 4243–4245. https://doi.org/10.1073/pnas.1603570113

Hansen, J., & Nazarenko, L. (2003). Soot climate forcing via snow and ice albedos. *Proceedings of the National Academy of Sciences*, *101*(2), 423–428. https://doi.org/10.1073/pnas.2237157100

Hirdman, D., Burkhart, J. F., Sodemann, H., Eckhardt, S., Jefferson, A., Quinn, P. K., et al. (2010). Long-term trends of black carbon and sulphate aerosol in the arctic: Changes in atmospheric transport and source region emissions. *Atmospheric Chemistry and Physics*, *10*(19), 9351–9368. https://doi.org/10.5194/acp-10-9351-2010

Hirdman, D., Sodemann, H., Eckhardt, S., Burkhart, J. F., Jefferson, A., Mefford, T., et al. (2010). Source identification of short-lived air pollutants in the arctic using statistical analysis of measurement data and particle dispersion model output. *Atmospheric Chemistry and Physics*, *10*(2), 669–693. https://doi.org/10.5194/acp-10-669-2010

Ikeda, K., Tanimoto, H., Sugita, T., Akiyoshi, H., Kanaya, Y., Zhu, C., & Taketani, F. (2017). Tagged tracer simulations of black carbon in the arctic: Transport, source contributions, and budget. *Atmospheric Chemistry and Physics*, *17*(17), 10515–10533. https://doi.org/10.5194/acp-17-10515-2017

Kanamitsu, M. (1989). Description of the NMC global data assimilation and forecast system. *Weather and Forecasting*, *4*(3), 335–342. https://doi.org/10.1175/1520-0434(1989)004<0335:DOTNGD>2.0.CO;2

Klimont, Z., Kupiainen, K., Heyes, C., Purohit, P., Cofala, J., Rafaj, P., et al. (2017). Global anthropogenic emissions of particulate matter including black carbon. *Atmospheric Chemistry and Physics*, *17*(14), 8681–8723. https://doi.org/10.5194/acp-17-8681-2017

Koch, D., & Genio, A. D. D. (2010). Black carbon semi-direct effects on cloud cover: Review and synthesis. *Atmospheric Chemistry and Physics*, *10*(16), 7685–7696. https://doi.org/10.5194/acp-10-7685-2010

Mauritsen, T. (2016). Greenhouse warming unleashed. *Nature Geoscience*, *9*(4), 271–272. https://doi.org/10.1038/ngeo2677

Navarro, J. C. A., Varma, V., Riipinen, I., Seland, Ø., Kirkevåg, A., Struthers, H., et al. (2016). Amplification of arctic warming by past air pollution reductions in Europe. *Nature Geoscience*, *9*(4), 277–281. https://doi.org/10.1038/ngeo2673

Petzold, A., Ogren, J. A., Fiebig, M., Laj, P., Li, S.-M., Baltensperger, U., et al. (2013). Recommendations for reporting "black carbon" measurements. *Atmospheric Chemistry and Physics*, *13*(16), 8365–8379. https://doi.org/10.5194/acp-13-8365-2013

Raes, F., Dingenen, R. V., Vignati, E., Wilson, J., Putaud, J.-P., Seinfeld, J. H., & Adams, P. (2000). Formation and cycling of aerosols in the global troposphere. *Atmospheric Environment*, *34*(25), 4215–4240. https://doi.org/10.1016/S1352-2310(00)00239-9

Randerson, J., Van der Werf, G., Giglio, L., Collatz, G., & Kasibhatla, P. (2017). Global fire emissions database, version 4.1 (gfedv4). ORNL Distributed Active Archive Center. https://doi.org/10.3334/ORNLDAAC/1293

Rastigejev, Y., Park, R., Brenner, M. P., & Jacob, D. J. (2010). Resolving intercontinental pollution plumes in global models of atmospheric transport. *Journal of Geophysical Research*, *115*, D02302. https://doi.org/10.1029/2009jd012568

Sand, M., Berntsen, T. K., von Salzen, K., Flanner, M. G., Langner, J., & Victor, D. G. (2015). Response of arctic temperature to changes in emissions of short-lived climate forcers. *Nature Climate Change*, *6*(3), 286–289. https://doi.org/10.1038/nclimate2880

Sato, Y., Miura, H., Yashiro, H., Goto, D., Takemura, T., Tomita, H., & Nakajima, T. (2016). Unrealistically pristine air in the arctic produced by current global scale models. *Scientific Reports*, *6*(26561). 1–9. https://doi.org/10.1038/srep26561

Schacht, J., Heinold, B., Quaas, J., Backman, J., Cherian, R., Ehrlich, A., et al. (2019). The importance of the representation of air pollution emissions for the modeled distribution and radiative effects of black carbon in the arctic. *Atmospheric Chemistry and Physics*, *19*(17), 11159–11183. https://doi.org/10.5194/acp-19-11159-2019

Schmeisser, L., Backman, J., Ogren, J. A., Andrews, E., Asmi, E., Starkweather, S., et al. (2018). Seasonality of aerosol optical properties in the arctic. *Atmospheric Chemistry and Physics*, *18*(16), 11599–11622. https://doi.org/10.5194/acp-18-11599-2018

Serreze, M. C., & Barry, R. G. (2011). Processes and impacts of arctic amplification: A research synthesis. *Global and Planetary Change*, *77*(1–2), 85–96. https://doi.org/10.1016/j.gloplacha.2011.03.004

Serreze, M. C., & Meier, W. N. (2018). The Arctic's Sea ice cover: Trends, variability, predictability, and comparisons to the Antarctic. *Annals of the New York Academy of Sciences*, *1436*(1), 36–53. https://doi.org/10.1111/nyas.13856

Serreze, M. C., & Stroeve, J. (2015). Arctic sea ice trends, variability and implications for seasonal ice forecasting. *Philosophical Transactions of the Royal Society A: Mathematical, Physical & Engineering Sciences*, *373*(2045), 20140159. https://doi.org/10.1098/rsta.2014.0159

Sharma, S., Ishizawa, M., Chan, D., Lavoué, D., Andrews, E., Eleftheriadis, K., & Maksyutov, S. (2013). 16-year simulation of arctic black carbon: Transport, source contribution, and sensitivity analysis on deposition. *Journal of Geophysical Research: Atmosphere*, *118*(2), 943–964. https://doi.org/10.1029/2012jd017774

Stein, A. F., Draxler, R. R., Rolph, G. D., Stunder, B. J. B., Cohen, M. D., & Ngan, F. (2015). NOAA's HYSPLIT atmospheric transport and dispersion modeling system. *Bulletin of the American Meteorological Society*, *96*(12), 2059–2077. https://doi.org/10.1175/BAMS-D-14-00110.1

Stohl, A. (2006). Characteristics of atmospheric transport into the Arctic troposphere. *Journal of Geophysical Research*, *111*, D11306. https://doi.org/10.1029/2005JD006888

Stohl, A., Klimont, Z., Eckhardt, S., Kupiainen, K., Shevchenko, V. P., Kopeikin, V. M., & Novigatsky, A. N. (2013). Black carbon in the Arctic: The underestimated role of gas flaring and residential combustion emissions. *Atmospheric Chemistry and Physics*, *13*(17), 8833–8855. https://doi.org/10.5194/acp-13-8833-2013

Willis, M. D., Leaitch, W. R., & Abbatt, J. P. (2018). Processes controlling the composition and abundance of arctic aerosol. *Reviews of Geophysics*, *56*(4), 621–671. https://doi.org/10.1029/2018rg000602

Winiger, P., Andersson, A., Eckhardt, S., Stohl, A., Semiletov, I. P., Dudarev, O. V., et al. (2017). Siberian arctic black carbon sources constrained by model and observation. *Proceedings of the National Academy of Sciences*, *114*(7), E1054–E1061. https://doi.org/10.1073/pnas.1613401114

Winiger, P., Barrett, T. E., Sheesley, R. J., Huang, L., Sharma, S., Barrie, L. A., et al. (2019). Source apportionment of circum-arctic atmospheric black carbon from isotopes and modeling. *Science Advances*, *5*(2), eaau8052. https://doi.org/10.1126/sciadv.aau8052